Supporting Information

Hafner et al. 10.1073/pnas.1008365107

SI Materials and Methods

Patients and Samples. In total, 175 SK from 25 patients (13 male and 12 female) were analyzed [16 Spanish (S) patients with 128 SK and 9 German (G) patients with 47 SK; average seven lesions/patient]. Age of appearance of the first SK ranged from 15 to 70 y (mean age, 48 y). The total number of SK was estimated by visual examination: Five patients had 10–25 SK, 2 patients had 25–50 SK, 9 patients had 50–100 SK, and 9 patients had >100 SK. SK were removed by curettage; half were immediately frozen in liquid nitrogen and stored, and the other half were formalin fixed and embedded in paraffin. The characteristics of the patients and SK are shown in Dataset S1.

Pathological Assessment. A single dermatopathologist (C.H.) assessed all SK according to uniform criteria. There were 105 acanthotic, 54 hyperkeratotic, and 16 adenoid SK. The proportion of hyperkeratotic SK was higher among the Spanish than among the German patients (36% vs. 17%, $P = 0.017$), in contrast to the proportion of acanthotic SK (52% vs. 81%, $P = 0.001$).

Mutational Analyses. DNA was isolated from frozen tissue after proteinase K digestion using the Qiagen DNeasy Mini Kit. *FGFR3* was investigated using a multiplex SNaPshot assay covering 11 hotspot mutations as described previously (1). A second independent PCR was used for confirmation. *PIK3CA* (E542K, E545G, E545K, H1047L, H1047R, and H1047Y), *HRAS* (G12A, G12C, G12D, G12S, G12V, Q61K, Q61L, and Q61R), and *PTPN11* (D61V, D61Y, E69K, A72T, A72V, E76G, and E76K) hotspot mutations were analyzed by Sequenom, using assays specifically designed for this project (information available upon request). A subset of all mutations was confirmed by direct sequencing of PCR products. *AKT1* mutations were detected by direct sequencing of exon 4 and confirmed by a second independent PCR. *TSC1* exons 3–23 were screened by heteroduplex analysis of PCR products (Light Scanner; Idaho Technology), as described elsewhere (2). Samples with an aberrant melting curve were sequenced and mutations were confirmed by a second PCR. For *PTEN*, exons 1–9 were amplified and analyzed using denaturing high performance liquid chromatography (DHPLC) (Transgenomics). PCR products showing abnormal DHPLC behavior were sequenced directly. In one patient, a germ-line *PTEN* intron 3 deletion (g.68202_68206del CTTTT) of unknown functional relevance was identified. Primer sequence and PCR conditions of all investigated genes can be obtained from the authors. A subgroup of 14 SK without mutations in the above-mentioned genes were analyzed by a highly sensitive genotyping assay (OncoCarta Panel v1.0; Sequenom), comprising 238 mutations in 19 oncogenes (*ABL1*, *AKT1*, *AKT2*, *BRAF*, *CDK*, *EGFR*, *ERBB2*, *FGFR1*, *FGFR3*, *FLT3*, *HRAS*, *JAK2*, *KIT*, *KRAS*, *MET*, *NRAS*, *PDGFRA*, *PIK3CA*, and *RET*) (3). A subset of the mutations identified in these assays was subsequently confirmed using standard PCR amplification and direct sequencing of PCR products. *KRAS* exon 2 mutations were analyzed in an additional panel of 45 SK harboring mutations in *FGFR3* ($n = 15$), *PIK3CA* ($n = 15$), or neither of these genes ($n = 15$).

Functional Analysis of TSC1 G1528C (D510H) Mutation. To assess the effect of this variant on protein levels, the G1528C mutation was introduced by site-directed mutagenesis in frame with a C-terminal FLAG-tag as described (2). *TSC1* wild-type and mutant retroviruses were produced to transduce *TSC1*-null urothelial cell lines HCV29 and 97-1 (4). Protein expression was analyzed in stably transduced cell pools as described (2), using anti-Hamartin (Invitrogen), anti-FLAG M2 (Stratagene), and anti-Tubulin (Serotec) antibodies and chemoluminiscence. Quantitation was performed using a Bio-Rad GelDoc system and Quantity One software.

To assess the effect of the G1528C variant on splicing, RNA was retrotranscribed using random hexamers. To detect alternatively spliced transcripts, fragments spanning exons 14–15 and 14–17 were amplified using primers 14F GTGATCTGGCCTCTGAAGAAGATAGT and TSC1 15BR AGCTCCTTGCTGTGCGCGTCT or 17R AGGGCATGCTGCTGCCTCTTA, respectively, and PCR products were separated by agarose gel electrophoresis.

Array Comparative Genomic Hybridization (aCGH). Twenty SK (two lesions per patient) and the corresponding leukocyte germ-line DNA from the same individual were analyzed. DNAs were differentially labeled with the genomic DNA Labeling Kit Plus from Agilent Technologies. All samples were hybridized against double-color Human Genome CGH 4 × 44k (Agilent Technologies), spanning the entire human genome at a median resolution of 75 kb. Hybridizations were done according to the manufacturer's protocols. Arrays were scanned using an Agilent DNA Microarray scanner G2565CA (Agilent Technologies). Microarray data were extracted with Feature Extraction Software v.9.6. All of the samples were considered for the study after filtering for quality of hybridization according to the quality control parameter (DLRSpread) provided by DNA Analytics v4.0.76. Data analysis and chromosome segmentation were performed using DNA Analytics and the Aberration Detection Method 2 (AMD-2) algorithm to identify all aberrant intervals in the samples. Alterations in copy number in five or more consecutive probes with a 10% minimum of penetrance were scored as aberrations.

X Chromosome Inactivation Analysis. The human androgen receptor allele-specific PCR assay was used. Genomic DNA (1 μg) was digested with 10 units of DdeI in 1× buffer 4 for 3 h at 37 °C and an aliquot was digested with methylation-sensitive enzyme HpaII or HhaI. A sham reaction was prepared without enzyme. After overnight incubation at 37 °C, digestion was terminated by heating at 65 °C for 20 min. Human androgen receptor (AR) allele-specific PCR was performed using fluorescein amidite (FAM)-labeled primers: TCCAGAATCTGTTCCAGAGCGTGC and GCTGTGAAGGTTGCTGTTCCTCAT (5). PCR was performed using HpaII- or HhaI-digested, or nondigested, DNA as template. PCR products were analyzed using the ABI 3130 Genetic Analyzer and the peak area was used to calculate the ratio of amplification of each allele before and after digestion.

Immunohistochemical Analyses of Proliferation, Senescence, and Signaling Markers. Tissue macroarrays (TMaA) were constructed using a 3-mm diameter punch as described (6). Each TMaA contained 16–21 SK and two to three samples of normal skin. Sections from paraffin-embedded tissues or TMaA were deparaffinized and processed for immunohistochemistry using either the Envision immunoperoxidase or alkaline phosphatase assays (Dako). The following antibodies were used: p14 (Ab-4; Neomarkers), p16 (Dako), p53 (DO7; Novocastra), Dec1 (rabbit polyclonal from A. Harris, Cancer Research UK, Oxford), HP-1γ (MAB3450; Chemicon International-Millipore), H3K9me3

(rabbit polyclonal, 07-442; Upstate Biotechnology), JUNB (C-11; Santa Cruz Biotechnology), Ki67 (MIB1; Dako), activated caspase 3 (JMH-62; Novocastra), 53BP1 (Novus), phospho-histone H3 (sc-8656-R; Santa Cruz Biotechnology), γ-H2AX (clone JBW301; Millipore), phospho-ERK1/2 (rabbit polyclonal; Cell Signaling Technology), and phosphor-p70S6 kinase (clone 1A5; Cell Signaling Technology). For some experiments, a comparison with a tissue microarray containing 38 squamous cell carcinomas was performed, as indicated. Immunostaining was scored according to the intensity (0–3) by two independent observers who reached consensus in cases of disagreement.

Western Blotting Analysis of Downstream Signaling in Normal Skin and SK. Normal skin was obtained from age-matched individuals or from the same cases with SK. Frozen sections were cut and the epidermis was manually microdissected for protein extraction; SK frozen sections were also used for protein extraction. Tissues were lysed in glycerol buffer [0.15 M Tris·HCl (pH 6.8), 5% SDS, 30% glycerol] diluted (1:3) in Nonidet P-40 buffer [25 mM Tris·HCl (pH 8.3), 50 mM NaCl, 0.5%Nonidet P-40, 0.5% sodium deoxycholate, 0.1% SDS] containing protease and phosphatase inhibitors. Samples were boiled 5 min before a 30-s sonication pulse. Proteins (70 μg) were fractionated in SDS/PAGE gels, transferred, and assayed for signaling markers of interest using standard procedures. The following antibodies were used: ERK1/2 (9102; Cell Signaling Technology), phospho-ERK1/2 (9101; Cell Signaling Technology), AKT1/2 (Sc-1619; Santa Cruz Biotechnology), phospho-AKT (9271; Cell Signaling Technology), GSK-3β (610202; BD Transduction Laboratories), phospho-GSK-3β (9323; Cell Signaling Technology), 4E-BP1 (9644; Cell Signaling Technology), phospho-4E-BP1 (2855; Cell Signaling Technology), p70S6 kinase (9202; Cell Signaling Technology), phospho-p70S6 kinase (9205; Cell Signaling Technology), and β-actin (clone AC-15; Sigma-Aldrich). Reactions were developed using chemoluminiscence (ECL; Amersham). For relative quantification, band intensities were analyzed using ImageJ software. Relative levels of phosphorylated proteins were determined using both the total corresponding protein and β-actin as reference because, for some of them, important changes in total protein were observed accompanying changes in the phosphorylation events when comparing SK with normal epidermis.

Statistical Analyses. Comparison of immunostaining in normal skin and SK was performed using the Mann–Whitney *U* test and Fisher's exact test. To assess the independence of two categorical variables, the χ^2 test was applied. To estimate the probability that clustering of lesions harboring the same mutation happens in a single subject, we computed the potential of the probability of a single mutation in the Spanish or the German population to the number of lesions in such individual. The overall probability was then estimated by multiplying the individual probabilities.

1. Hafner C, et al. (2006) Mosaicism of activating FGFR3 mutations in human skin causes epidermal nevi. *J Clin Invest* 116:2201–2207.
2. Pymar LS, Platt FM, Askham JM, Morrison EE, Knowles MA (2008) Bladder tumour-derived somatic TSC1 missense mutations cause loss of function via distinct mechanisms. *Hum Mol Genet* 17:2006–2017.
3. Thomas RK, et al. (2007) High-throughput oncogene mutation profiling in human cancer. *Nat Genet* 39:347–351.
4. Knowles MA, Habuchi T, Kennedy W, Cuthbert-Heavens D (2003) Mutation spectrum of the 9q34 tuberous sclerosis gene TSC1 in transitional cell carcinoma of the bladder. *Cancer Res* 63:7652–7656.
5. Allen RC, Zoghbi HY, Moseley AB, Rosenblatt HM, Belmont JW (1992) Methylation of HpaII and HhaI sites near the polymorphic CAG repeat in the human androgen-receptor gene correlates with X chromosome inactivation. *Am J Hum Genet* 51:1229–1239.
6. Fernández PL, et al. (2003) Easier tissue macroarray ("microchop") production. *Appl Immunohistochem Mol Morphol* 11:365.

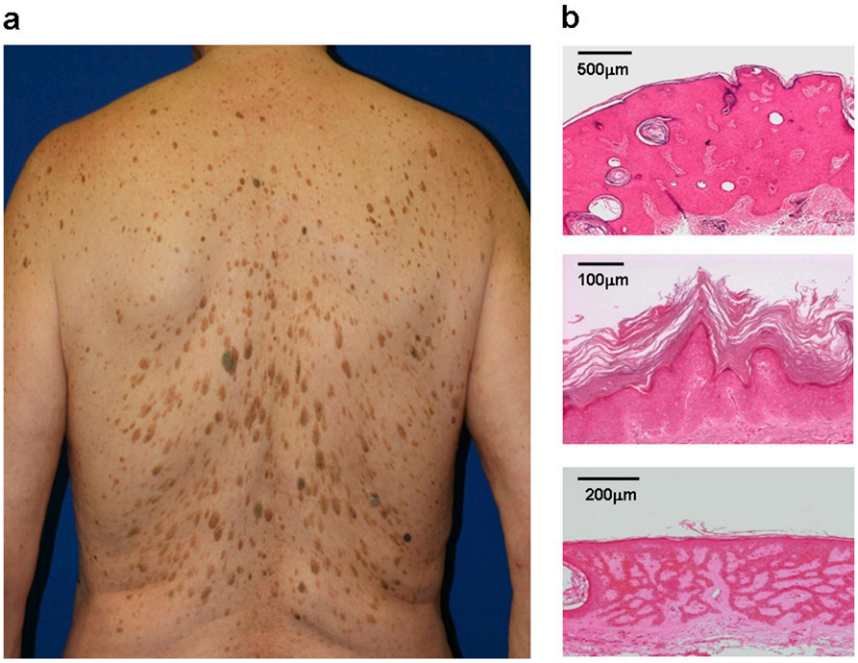

Fig. S1. Macroscopic and microscopic aspect of seborrheic keratosis (SK). (*A*) A patient displaying multiple SK in the back. (*B*) Histological appearance of acanthotic (*Top*) and hyperkeratotic and adenoid (*Middle* and *Bottom*) SK.

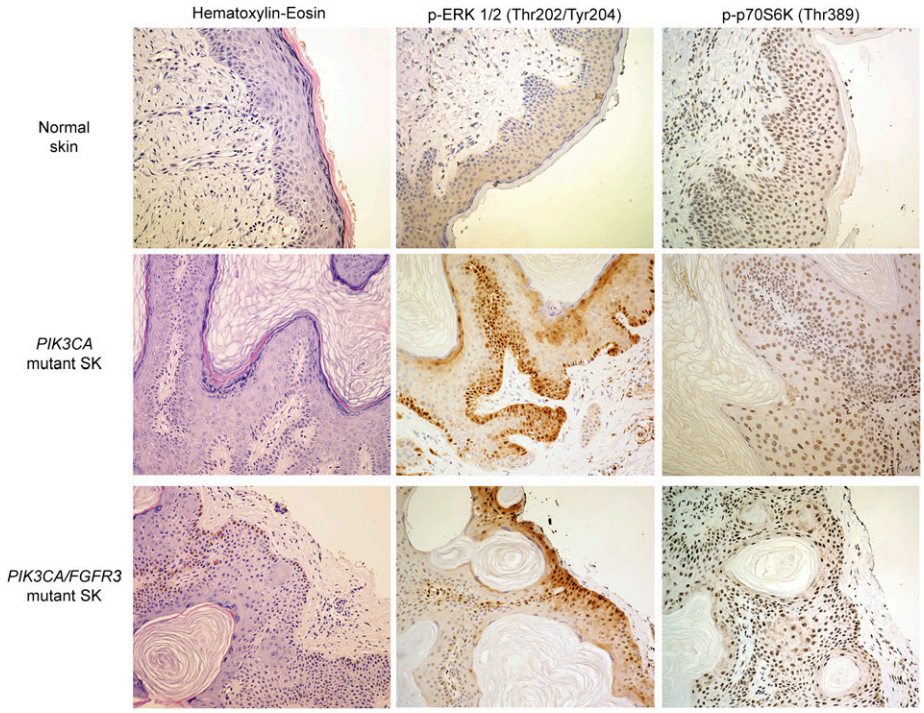

Fig. S2. Immunohistochemical analysis of p-ERK1/2 and p-p70S6K in normal skin and in two SK. A clear increase in p-ERK1/2 signal, mainly in the basal region of the epidermis, is observed in SK. By contrast, there was no consistent difference in p-p70S6K staining intensity.

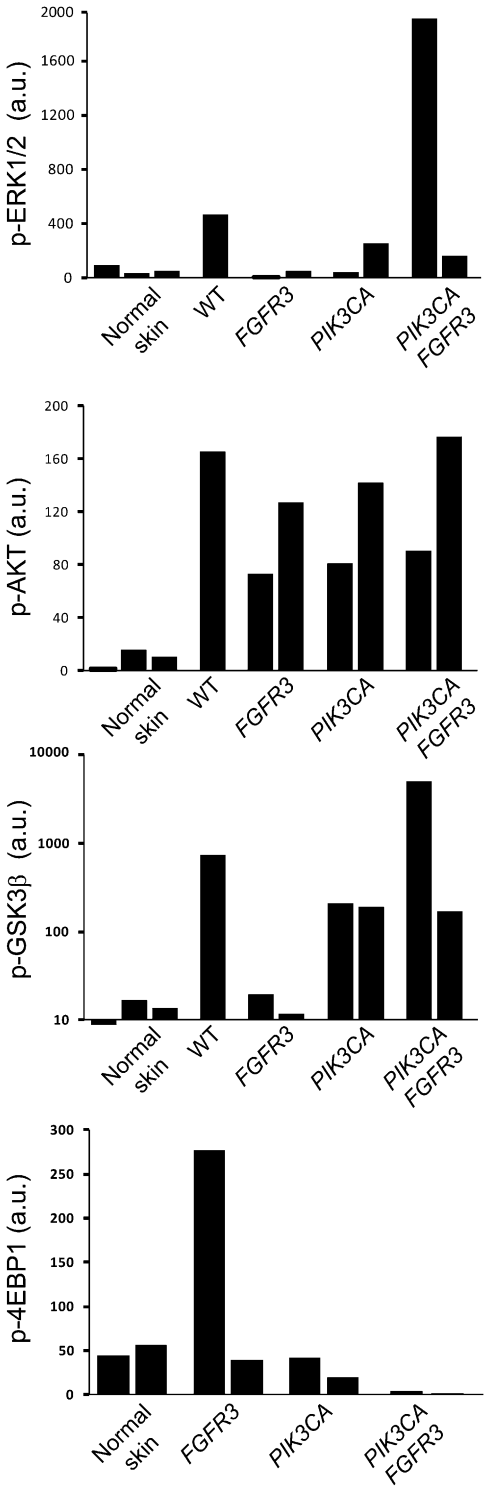

Fig. S3. Densitometric quantitation analysis of Western blotting results shown in Fig. 4.

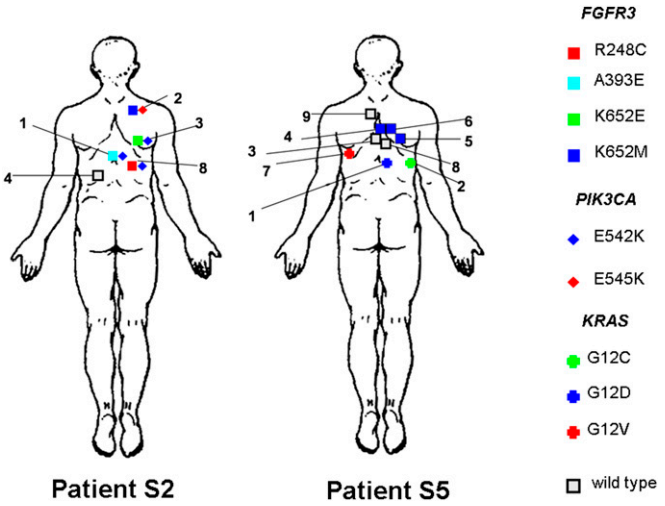

Fig. S4. Distribution and genotypes of SK in patients S2 and S5.

Dataset S1. Clinical characteristics of patients and SK

Dataset S1 (XLS)

Dataset S2. Detailed results of mutational analyses

Dataset S2 (XLS)